Available online at www.sciencedirect.com

ScienceDirect

Geochimica et Cosmochimica Acta 333 (2022) 124–135

Geochimica et Cosmochimica Acta

www.elsevier.com/locate/gca

Multi-element constraints on the sources of volatiles to Earth

Z.D. Sharp, P.L. Olson

Department of Earth and Planetary Sciences, Northrop Hall, 1 University Ave., University of New Mexico, Albuquerque, NM 87131, USA

Received 17 January 2022; accepted in revised form 4 July 2022; Available online 12 July 2022

Abstract

A number of studies have used one or several isotopic systems to estimate the origin of Earth's volatiles. Several volatile sources and subsequent volatile loss are generally considered in these models. In this communication, we use a forward model based on the presumed formation history of Earth to simultaneously constrain the sources for seven volatile elements (H, He, N, Ne, Ar, Kr and Xe). We consider the three potential volatile sources: nebular ingassing, chondrites, and comets. Sinks include loss by early hydrodynamic escape and long-term loss of ionized Xe. 10,000 Monte Carlo simulations generate several hundred solutions that match the abundance of all these elements to within a factor of ~2 of the present-day Earth values, as well as critical isotope ratios ($\delta^{15}N$, $^{20}Ne/^{22}Ne$, $^{36}Ar/^{38}Ar$, Kr and Xe). The source of volatiles is distinctly different for different elements. Our results indicate that there was a large excess of H, He and Ne supplied by nebular ingassing, with subsequent massive loss (>99% He and Ne) by early hydrodynamic escape. Kr and Xe were supplied primarily by comets, and N was supplied almost entirely (>98%) by chondrites. The source of Ar is mixed, with 50–90% chondrites and the remainder from ingassing. Solutions with nitrogen isotope ratios that match Earth values require a > 92% E chondrite source. $\delta^{15}N$ values are far too high using a C chondrite source (>20‰ vs AIR). Our results suggest late addition of $7.5 \pm 0.7 \times 10^{21}$ g comets, $8.3 \pm 5.6 \times 10^{24}$ g C chondrites and $1.2 \pm 0.5 \times 10^{26}$ g E chondrites.

The Kr isotope pattern should follow that of cometary input, given that > 90% of all Kr comes from a comet source. Our results fit the measured values of Comet 67P/C-G within error. Xe isotope data can be matched to Earth values using solar isotope values as an assumed cometary source if we assume a large mass-dependent enrichment factor during loss of ionized Xe to space. The measured isotope data for Comet 67P/C-G have both light and heavy Xe isotope ratios that do not match the Earth atmosphere data, suggesting that this comet is not, in our model, representative of the Earth cometary Xe source.

The amount of ingassed H is critically dependent on oxygen fugacity, ranging from 11 to 22 times the present day ocean amount for presumed low $f(O_2)$ of the early magma ocean. Even at low $f(O_2)$ values, most of the water is dissolved as H_2O rather than H. A large hydrogen isotope fractionation during hydrodynamic escape ($\alpha = 1.6$ to 1.7) is required to explain the present-day D/H values. This α value corresponds to equilibrium between H_2 and H_2O at ~300 °C or loss of atomic H to space. Loss of hydrogen early in Earth's history easily accounts the relatively high $f(O_2)$ of Earth's present-day mantle.

Keywords: Nebular ingassing; Source of volatiles; Noble gases; Planetary formation

1. INTRODUCTION

The sources of volatiles to Earth are poorly constrained. In the classical 'Safronov' growth model (Safronov, 1972; Wetherill, 1980) it is assumed that the Earth formed inside the 'snow-line', defined as the region where the solar nebula dissipated before temperatures dropped sufficiently for volatiles to condense. As a result, volatiles could not have accreted as ices on the growing proto-Earth. In light of these considerations, three potential volatile sources are generally considered: addition from chondrites, addition from comets, and direct ingassing from a nebular

E-mail address: zsharp@unm.edu (Z.D. Sharp)

https://doi.org/10.1016/j.gca.2022.07.007
0016-7037/

atmosphere. Solar wind implantation has also been considered as a potential source for mantle He, Ne and Ar (Péron et al., 2017), with subtle differences in isotope ratios from direct ingassing. Models generally consider one or two of these potential sources, with several elemental abundances and isotope ratios as constraints (e.g., Zhang and Zindler, 1989; Harper and Jacobsen, 1996; Dauphas and Marty, 2002; Holland et al., 2009; Marty, 2012; Halliday, 2013; Moreira, 2013; Caracausi et al., 2016; Hirschmann, 2016; Williams and Mukhopadhyay, 2018; McCubbin and Barnes, 2019; Bekaert et al., 2020). In addition to sources, a number of loss mechanisms or 'sinks' have been recognized, including hydrodynamic escape (Zahnle and Kasting, 1986; Hunten et al., 1987; Marty, 2012; Zahnle et al., 2019), impact erosion (Genda and Abe, 2005), and sequestration to the deep mantle and core (Wu et al., 2018; Roth et al., 2019). Typically, inverse model approaches estimate the contribution from each source in order to get a best-fit to the measured data. In this communication, we use a forward model approach, which generates the final Earth composition without any *a priori* constraints. Our mass balance model simultaneously considers the volatile species, H, He, N, Ne, Ar, Kr and Xe for abundances and isotope ratios. We limit the model to bulk Earth concentrations and isotope ratios, and do not detail the differences between the mantle and atmospheric reservoirs for these rare gases (se, for example Moreira, 2013).

2. MODEL PROTOCOL

Our simplified mass balance model is structured around the presumed formation history of the Earth. In the first few million years following the collapse of the presolar molecular cloud, the Earth grew in the presence of the nebular disk. The growth mechanism could either be stochastic, by incorporation of ever larger planetesimals and planetary embryos (O'Brien et al., 2014; Walsh and Levison, 2016), or continuous, by rapid accumulation of small 'pebble-size' objects (Levison et al., 2015; Johansen and Lambrechts, 2017; Johansen et al., 2021). Once a planet exceeds ~0.25 Earth masses (M_E), it will develop a thick atmosphere and magma ocean, and begin ingassing material from the nebula. The amount of ingassed material for Earth has been calculated previously (Olson and Sharp, 2019) and is used as the initial source of volatiles to Earth.

After dissipation of the nebula, the nebular atmosphere disperses, atmospheric pressures decrease and degassing of the silicate magma occurs. This second phase results in atmospheric erosion which leads to hydrodynamic escape of volatiles (Zahnle and Kasting, 1986; Hunten et al., 1987).

A final phase of volatile delivery comes from late addition of comets and chondrites. Late addition of chondritic material was originally proposed to satisfy the high concentrations of highly siderophile elements in the Earth's mantle (Chou, 1978; Walker, 2009). It has subsequently been suggested that late addition is also a major source for volatiles (Dauphas and Marty, 2002; Marty, 2012; Albarede et al., 2013).

Lastly, we assume that there was a long-term loss of Xe *via* non-thermal ionization escape. Xe is the most easily ionized noble gas, and it is postulated that ionized Xe can be lost through the polar wind (Marty, 2012; Hébrard and Marty, 2014; Zahnle et al., 2019). Evidence for preferential loss of Xe through time has been suggested by numerous authors both for the Earth (Pujol et al., 2011; Avice and Marty, 2020) and Mars (Cassata et al., 2022).

3. SOURCES AND SINKS OF VOLATILES

3.1. Nebular ingassing

If planetary growth occurs in the presence of a stellar nebula, a thick atmosphere will develop once a planet exceeds ~0.25 Earth mass (Olson and Sharp, 2019). At that point, surface temperatures surpass the basalt solidus, which results in dissolution of the atmospheric gases into the silicate magma ocean (Hayashi et al., 1985). Our ingassed estimates for H_2, He, N, Ar, Kr, and Xe follow the methods of Olson and Sharp (2018; 2019). In this work, we estimate ingassing based on presumed the solar nebula composition (e.g., Lodders, 2003; Marty et al., 2011; Heber et al., 2012) rather than using Jovian atmospheric abundances as was done in our previous work.

The amount of ingassed material is primarily controlled by the duration, or 'lifetime', of the solar nebula relative to the planet accretion time. Calculated ingassed abundances of H, He, N, Ne, Ar, Kr and Xe for a (nebula lifetime)/(accretion time) ratio of 0.5 are given in Table 1 using proto-solar abundances and early solar system nuclide abundances. Such conditions would be equivalent to the solar nebula persisting for 5 My and 90% Earth accretion by 10 My (or in general, any reasonable 2/1 ratio of accretion time/duration of solar nebula).

There is no hard constraint on the lifetime of the solar nebula, although published studies provide some estimates. There is a general consensus that chondrules formed in the presence of a nebular gas (Desch and Connolly, 2002). Chondrule ages extend to slightly more than 4 My after solar system formation (Villeneuve et al., 2009; Bollard et al., 2017). This provides a minimum duration time for the nebular gas. If the nebular solids (chondrules or pebbles) cleared prior to the gas nebula, as expected during radial inward drift due to the sub-Keplerian velocities of the solids (Johansen et al., 2021), then the gas could have persisted without chondrule formation for an even longer time. Age estimates for the solar nebula can also be constrained from observations of optically thick disks surrounding T Tauri stars. Stars with an age of ~3 My after formation have a 50% disk frequency, with some star clusters still having disk frequencies of 10–20% at 10 My (Hernandez et al., 2007). We conclude that a minimum duration of 4–6 My for the solar nebula is reasonable in light of the above information.

The growth rate of the Earth is also poorly constrained. Hf-W and U-Pb isotope data provide some bounds. A reasonable fit to an exponentially decreasing growth rate model given by is obtained with a τ value = 2.75 My (Kleine and Walker, 2017). This corresponds to 90%

Table 1
Calculated volatile additions from direct ingassing (row 1), chondrite and cometary additions (rows 2 and 3), present-day estimates (rows 4–11) and our model Earth abundances (row 12), which includes the contributions from ingassing, comets and chondrites as well as loss by hydrodynamic escape. Parentheses indicate 1σ errors.

Moles in Earth	H	^{3}He	^{14}N	^{20}Ne	^{36}Ar	^{84}Kr	^{130}Xe
Amount ingassed [1]	2.5×10^{24}	5.2×10^{17}	7.1×10^{17}	2.0×10^{18}	1.4×10^{15}	3.2×10^{12}	1.1×10^{10}
Chondrite addition[†]	(3.2–20) $\times 10^{22}$		1.2 (0.3) $\times 10^{21}$	6.5 (1.8) $\times 10^{14}$	3.6 (1.0) $\times 10^{14}$	2.1 (0.6) $\times 10^{13}$	2.7 (0.9) $\times 10^{12}$
comet addition[†]	(2.0–3.6) $\times 10^{20}$		1.0 (0.1) $\times 10^{19}$	2.2 (0.7) $\times 10^{14}$	4.8 (5.0) $\times 10^{14}$	1.0 (0.6) $\times 10^{14}$	1.0 (0.9) $\times 10^{12}$
Earth [2]	1.4×10^{24}	1.6×10^{14}	7.7×10^{20}	3.0×10^{15}	5.6×10^{15}	1.2×10^{14}	6.8×10^{11}
Earth [3]	1.7×10^{24}		6.8×10^{20}	1.9×10^{15}	5.9×10^{15}	1.2×10^{14}	7.4×10^{11}
Earth [4]	5.2×10^{23}		6.7×10^{20}	2.9×10^{15}	5.5×10^{15}	1.1×10^{14}	6.3×10^{11}
Earth [5]	1.9×10^{23}		3.9×10^{20}	3.0×10^{15}	5.7×10^{15}	1.2×10^{14}	6.4×10^{11}
Earth [6]		1.9×10^{12}					
Earth [7]	0.2–1.3×10^{24}	0.3–2.2×10^{14}	4.3–7.8×10^{20}	2.9–3.3×10^{15}	5.7–6.6×10^{15}	1.2–1.3×10^{14}	0.6–1.6×10^{12}
Undepleted mantle [8]		1.7×10^{14}					
Earth avg.	1.2×10^{24}	1.03×10^{13}	7.1×10^{20}	2.6×10^{15}	5.7×10^{15}	1.2×10^{14}	6.8×10^{11}
Model Earth abundances (this study)	1.7×10^{24}	7.90×10^{12}	4.8×10^{20}	3.0×10^{15}	1.0×10^{16}	1.2×10^{14}[‡]	6.8×10^{11}[‡]

[1](Olson and Sharp, 2019 corrected for solar abundances), [2](Halliday, 2013), [3](Marty, 2012), [4](Dauphas and Morbidelli, 2014), [5](Pepin, 1991) [6](Porcelli and Elliott, 2008), [7](Dauphas and Marty, 2002) [8](Porcelli and Ballentine, 2002).
[†] Calculated abundances to match Kr and Xe using equations (2) and (3).
[‡] Model requires Kr and Xe to match measured abundances (Equations (2) and (3)).

growth of Earth within 10 My after solar system formation. Another recent estimate based on iron isotope ratios suggest a formation age of Earth of 5 million years (Schiller et al., 2020). Changing the growth rate of Earth or changing the nebula lifetime by several million years will change the ingassed values in Table 1 by no more than a factor of 2. Recently a model of planetary growth by capture of small centimeter to meter size objects during their radially inward drift has been developed. This 'pebble accretion' model results in rapid growth, such that protoplanets can acquire Earth-like masses within a few million years (Levison et al., 2015; Johansen and Lambrechts, 2017; Ida et al., 2019; Johansen et al., 2021).

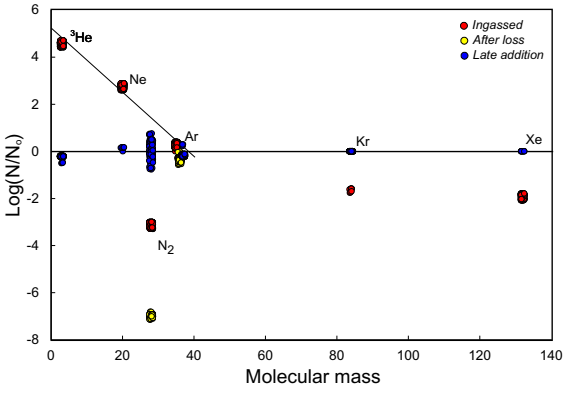

Fig. 1. Variations in the volatile abundance vs. molecular mass from a number of 'best-fit' simulations. The y-axis is the amount of element relative to the present day Earth abundance. Red circles are ingassed amounts, yellow circles are post-hydrodynamic escape amounts, and blue circles are final amounts following addition from chondrites and comets, less long-term Xe loss. Numerous best-fit solutions satisfy all element abundances.

Ingassed amounts are given in Table 1 and Fig. 1. In or model simulations, we treat the ingassing amounts as a free parameter, allowing it to vary between 1 and 100‰ of the estimate in Table 1. Accretion of volatile-bearing solids may have contributed to the initial volatile inventory of Earth. However, we assume that a substantial fraction of the early-accreted volatiles would be lost during hydrodynamic escape (Benedikt et al., 2020), and that the magma ocean would have mostly reached equilibrium with the high pressure atmosphere, such that the contribution from volatiles derived from accreting objects would have been overprinted by the ingassing volatiles.

3.2. Atmospheric erosion

Astronomical observations identify young stars either with or without nebular disks. Transitional disks are lacking, suggesting that the timescale for disk dispersal is rapid, on the order of 10^5 y (Alexander et al., 2014). When the solar nebula dissipated, the dense atmosphere surrounding the proto-Earth would have eroded away in a time span of several million years (Olson and Sharp, 2019). With the lower confining pressure, extreme mantle degassing would occur (Sekiya et al., 1980; Pepin, 1991; Porcelli and Elliott, 2008; Sharp, 2017).

Our time-integrated estimates for the amounts of light gases ingassed far exceeds the present-day abundances. There is a 10^4 excess of ^{3}He and 5×10^2 excess of ^{20}Ne compared to modern values (Table 1). The excess for hydrogen is $>10^{24}$ g. The loss of the excess hydrogen, following dispersal of the nebula, would have promoted efficient

hydrodynamic escape for the light noble gases (Zahnle and Kasting, 1986; Hunten et al., 1987).

3.3. Late addition from comets and chondrites

The concept of late delivery, or 'late accretion' of volatiles by chondrites was developed originally as an explanation for the anomalously high concentration of highly siderophile elements (HSE –Os, Ir, Ru, Rh, Pt, Pd, Re, Au) in the mantle (Chou, 1978; Drake and Righter, 2002). If early core formation scavenged the HSEs into the metal phase, the unexpectedly high measured HSE mantle abundance can be explained by addition of 0.3 to 1‰ M_E of chondritic material to Earth following core formation. If this late material was volatile rich (e.g., carbonaceous chondrites), it could account for many of the volatile elements as well (e.g., Javoy, 1998; Albarède, 2009).

The late accretion model is supported by the similar D/H ratio of Earth and carbonaceous chondrites, a presumed source of water in the late accretion model (Robert, 2001; Alexander et al., 2012). Whereas other sources, such as comets or nebular hydrogen have D/H ratios that are generally too high or too low, the D/H ratios of the carbonaceous chondrites (Robert et al., 2000; Alexander et al., 2012) broadly overlap the bulk Earth value of 149×10^{-6} (Lécuyer et al., 1997). Recent HSE isotope studies, however, indicate that non-carbonaceous chondrites, such as enstatite chondrites, provide the best fit to the Earth HSE inventory (Walker, 2009; Fischer-Gödde and Kleine, 2017; Carlson et al., 2018; Zhu et al., 2021). An enstatite chondrite source for late accretion would not provide a significant source of volatile elements, particularly H (see however, Piani et al., 2020).

3.4. Loss of Xe

In contrast to the light noble gases, Kr and Xe ingassing contributes at most a few percent of the present-day total inventory for these elements (Table 1). Additions of Kr and Xe from chondrites and comets by late addition are required to account for their present day abundances. Because their masses are well above the crossover mass (explained in following section), loss by hydrodynamic escape should have been minimal. However, Xe has the lowest ionization potential of the noble gases, and it has been proposed that the Xe isotope pattern on Earth is due to loss of ionized Xe to space (Marty, 2012; Hébrard and Marty, 2014; Avice et al., 2017; Zahnle et al., 2019). We therefore add a 'Xe-loss term', which is treated as a free parameter. In contrast to the heavy gases, any He, and to a lesser extent Ne, delivered by late addition would have been volatilized during impact (Tyburczy et al., 1986) and lost from the Earth system.

4. METHODS

Our forward model consists of the following three steps:

1. Gases are supplied to Earth by nebular ingassing. We treat the actual amount of ingassed material as a free parameter, allowing it to vary between 1% and 100% of our best estimate (Olson and Sharp, 2019). Ingassed amounts are shown in Fig. 1 by the red circles. There is a vast excess of He and Ne ingassed relative to present day abundances. There is a large deficit for N_2, and less than 1% of Kr and Xe are sourced by nebular ingassing.
2. The light volatiles H, He, N, Ne, and potentially Ar, are partially lost by hydrodynamic escape. Hunten et al. (1987) showed that during hydrodynamic escape, the log of the initial gas abundance divided by the final gas abundance varies linearly with mass. We follow the formulation of Hunten et al. (1987), where

$$\log_{10}(N_o/N) = a\mathrm{M} + b \quad (1)$$

to estimate the amounts of volatiles lost by hydrodynamic escape. In equation (1), N is the present-day abundance of a species on Earth, N_o is the amount ingassed and M is the mass of the species in amu. The crossover mass, given by $-b/a$, is the mass above which minimal hydrodynamic escape occurs. The constants a and b in this study are determined from the best fit to the concentration ratios $\log(N_o/N)$ of He, Ne and Ar (Fig. 1) with a best-fit crossover mass of 39 ± 3 amu, close to the atomic mass of Ar. This crossover mass implies that minimal Kr and Xe and only minor Ar were lost by hydrodynamic escape. The constants in equation (1) are generated automatically (based on assumed ingassed amounts) to obtain the best fit to the present-day abundances. There are no free parameters in this step. The elemental abundances remaining after loss are shown by the yellow circles in Fig. 1.

3. Late addition of comet and chondrites occurs followed by ionized Xe loss. Kr and Xe ingassing contributes at most a few percent of the present-day total inventory for these elements (Table 1, Fig. 1). The principal source for Kr and Xe is therefore assumed to be from chondrites and comets (Moreira et al., 1998). Because their masses are well above the crossover mass, loss by hydrodynamic escape should have been minimal. We do, however assume a protracted loss of ionized Xe from the polar wind. The amount of Xe loss is treated as a free parameter.
4. The amount of chondritic and cometary material necessary to satisfy the present-day mass balance for Kr and Xe can be determined by solving the following two coupled mass balance equations:

$$X_{Xe-ing} + x_{chon}C_{Xe-chon} + x_{com}C_{Xe-com} - X_{Xe-loss} = X_{Xe-Earth} \quad (2)$$

$$X_{Kr-ing} + x_{chon}C_{Kr-chon} + x_{com}C_{Kr-com} = X_{Kr-Earth} \quad (3)$$

where X_i is the moles of the element in component i, x_i is the amount of phase i (in grams), and C_i is the concentration of the element in phase i (in moles/g). *ing* is ingassed component, *chon* is chondrite component, *com* is cometary component, *loss* is the ionized Xe lost to space, and *x-Earth* is present-day abundance.

In equations (2) and (3), we are solving for the mass of late comet and chondrite addition. Three parameters are varied. The first is $X_{Xe\text{-}loss}$, the amount of Xe loss during ionization. The second is the isotopic composition of Xe, which we consider as equal to solar value (Meshik et al., 2007) or that measured in Comet 67P/C-G (Marty et al., 2017). The third is the type of chondrite added. We consider carbonaceous and enstatite chondrites as the two endmember value varying it between 100% C chondrite and 100% E chondrite.

4.1. Summary of model parameters and protocol

Our input data are compiled from multiple sources (see Tables 1 and S1-S3), and no attempt is made to assess the relative uncertainties of our input data, unless otherwise indicated. Our results are controlled by the following five free parameters:

Ingassed fraction: varied from 1 to 100% of our previous estimate (Olson and Sharp, 2019) modified for a presumed solar nebula composition.
The proportion of C and E chondrites: varied from 100 % C chondrites to 100% E chondrites.
The comet Xe isotope ratio: We run the model using the measured value from Comet 67P/C-G (Marty et al., 2017) and an assumed solar ratio (Meshik et al., 2007), recognizing that the composition of Comet 67P/C-G may not be representative of comets delivered to Earth.
The isotopic fractionation (the α value) associated with hydrodynamic escape of Xe: Fractionation is based on the equation $R = R_o \times F^{(\alpha-1)}$ where R and R_o are the initial and final $^{i}Xe/^{130}Xe$ values and α (given by $\sqrt{M_1/M_2}$) is varied as $x(\alpha\text{-}1) + \alpha$, where x ranges from 0 to 4. The results in a ~3‰ change in α.
The isotope fractionation associated with hydrodynamic escape of N, Ne and Ar: For these elements, we would expect that the isotope fractionation during hydrodynamic escape to follow the mass dependency given by equation (1). However, Benedikt et al. (2020) concluded that there is no isotopic fractionation for Ar and Ne if loss rates for these elements during hydrodynamic escape are high. We therefore consider the isotopic fractionation for N, Ne and Ar to range from zero (no fractionation) to the value predicted from equation (1).

5. RESULTS

The results of a 10,000 run Monte Carlo simulation are given in Appendix A. (Supp. Material Table S4). Of the 10,000 simulations, more than one half have non-physical solutions, such as negative chondrite additions or H abundances less than the present-day ocean equivalent (1.4×10^{24}g H_2O). Of the remaining solutions, there is no correlation of all variables towards a single best-fit. In other words, different combinations of variables are found to give equivalently good fits. In spite of the lack of convergence to a single best-fit solution, there are multiple solutions that result in final abundances of He, Ne, Ar and N_2 within a factor of 2 of the assumed modern-day values (Fig. 1). Estimated contributions from ingassing, comet, and chondrite delivery for H, He, N, Ne, Ar, Kr, and Xe are given in Table 1 using the average of 400 simulations that closely approach modern abundances. A summary of the best-fit values with uncertainties are shown in Table 2.

6. DISCUSSION

6.1. Sources

While there is no single best fit solution from our model simulations, there are a number of robust conclusions that can be made. Most notably, different volatiles clearly come from different sources (Fig. 2). He is overwhelming sourced from ingassing. Ne is primarily sourced from ingassing, with the remaining 25% from chondrites. Nitrogen is supplied almost entirely from chondrites, whereas Kr and Xe are primarily sourced from comets with the remainder from chondrites. Earth's argon is from chondrites and some ingassing. The fact that different volatiles have completely different sources has important implications for source identification and quantification.

The masses of chondrite and comet late delivery are shown in Fig. 3. The chondrite addition depends on the presumed final $\delta^{15}N$ value for a simulation (see following Section 6.2). For solutions that have the requisite negative $\delta^{15}N$ value matching present-day Earth, the chondrite late addition averages $1.3 \pm 0.5 \times 10^{26}$ g, averaging 2×10^{24} g C chondrite; 1.2×10^{26} g E chondrite). Average cometary addition is $7.5 \pm 0.7 \times 10^{21}$ g.

These abundances compare favorably with previous estimates for the cometary contribution (Marty et al., 2016; Bekaert et al., 2020). Previous chondrite abundance estimates are at the low end of our simulations. Dauphas and Marty (2002) suggest 0.7–2.7 $\times 10^{25}$ g of chondritic addition. Pepin (1991) proposes a late addition of 1.32×10^{25} g E chondrite and 3×10^{21} g cometary addition.

6.2. Nitrogen isotope constraints

Nitrogen is sourced almost entirely from chondrites (Fig. 2) with a very minor contribution from comets. The $\delta^{15}N$ value of the Earth should reflect that of the chondrite source (Our model considers only carbonaceous and enstatite chondrites). C chondrites (exclusive of CV chondrites, which have very low N concentrations) have an average $\delta^{15}N$ value of +20‰ (Grady and Wright, 2003; Pearson et al., 2006), while E chondrites have a significantly lower value averaging –18‰ (Grady et al., 1986; Patzer and Schultz, 2002). Cartigny and Marty (2013) estimate a bulk Earth $\delta^{15}N$ value of −4 to −1‰. In order to obtain a $\delta^{15}N$ value that matches the present-day Earth, more than 92% of the chondrite addition must come from E chondrites (Fig. 4). It is worth noting that hydrodynamic escape of N_2 would raise the $\delta^{15}N$ value of the remaining nitrogen. Unless there is some mechanism to lower the $\delta^{15}N$ value of the atmosphere, C chondrites are an unlikely candidate for the primary source of nitrogen to Earth. An E chondrite source has been suggested previously from volatile data

Table 2
Averages of 200 selected 'best-fit' solutions from 10,000 Monte Carlo simulations for volatile sources (row 1). A best fit solution that satisfies Xe isotope ratios as well is given in row 2, using an α value 3% greater than the ideal mass dependent fractionation into a vacuum. Numbers in parentheses indicate 1σ error.

H abundance (g)	Comet addition (g)	C chondrite (g)	E chondrite (g)	$\delta^{15}N$ ‰	$^{20}Ne/^{22}$	$^{36}Ar/^{38}Ar$	^{132}Xe lost (g)	Ingas fractionation*
Average of 200 'best fit' solutions								
$1.7(0.4) \times 10^{24}$	$7.5\ (0.7) \times 10^{21}$	$8.3(5.6) \times 10^{24}$	$1.2(0.5) \times 10^{26}$	-1.1 ± 0.7	9.8 ± 1.1	5.0 ± 0.2	$3.1(0.8) \times 10^{12}$	0.6 ± 0.2
Solution that matches Xe isotopes with α = 3.3 (shown in Fig. 8)								
1.9×10^{24}	7.3×10^{21}	1.3×10^{25}	1.1×10^{26}	−0.7	9.6	5.2	3×10^{12}	0.84

* Fractionation during hydrodynamic escape relative to value from equation (1).

(Lammer et al., 2020; Piani et al., 2020) and numerous studies using moderately and highly siderophile element isotope geochemistry (Walker et al., 2002; Fischer-Gödde and Kleine, 2017; Hopp and Kleine, 2018; Nanne et al., 2019).

6.3. Ne and Ar isotopes

Our calculated $^{20}Ne/^{22}Ne$ values overlap the present-day air value, while the calculated $^{36}Ar/^{38}Ar$ is generally less than the air value of 5.3, with a band of solutions that have $^{36}Ar/^{38}Ar$ ratios of ~5.5 (Fig. 5). The distinct clusters of $^{36}Ar/^{38}Ar$ values are related to the calculated crossover mass during hydrodynamic escape (equation (1)) and demonstrate the sensitivity of the $^{36}Ar/^{38}Ar$ ratio to this parameter. The $^{20}Ne/^{22}Ne$ ratios of our simulations average 9.85 ± 1.10, compared to air with a ratio of 9.78 and ocean island basalts averaging 12.5 (Trieloff et al., 2000). The distinct $^{20}Ne/^{22}Ne$ ratios between the atmosphere and mantle are explained in terms of inefficient recycling of Ne during subduction (Moreira et al., 2003; Péron et al., 2018). The high $^{20}Ne/^{22}Ne$ ratios of mantle samples is presumably from nebular ingassing (Yokochi and Marty, 2004; Williams and Mukhopadhyay, 2018) or Ne implanted from solar wind ions in meteorites (Trieloff et al., 2000). The lower $^{20}Ne/^{22}Ne$ values of the atmosphere are primarily explained by late addition of chondritic material.

6.4. Kr and Xe

We find that the majority of Earth's Kr was sourced by comets (Fig. 2). We do not consider isotope fractionation for Kr in our model, so that the Kr isotope trends should mimic the cometary source. Two Kr isotope ratios for comets are considered. One is the measured data for Comet 67P/C-G (Rubin et al., 2018), and the other is equal to solar values (Meshik et al., 2007) (Fig. 6). Errors on the measured Kr isotope ratios are relatively large and show an ^{83}Kr deficit compared to the solar ratios. This may be related to a ~5% addition of an s-process component (Rubin et al., 2018). Simulations fall into two groups, depending on whether the solar or measured Kr isotope ratio of comets is assumed (Fig. 6). The Earth Kr isotope values match both the measured input data and solar nebula input within error.

The abundances of ^{128}Xe, ^{129}Xe, ^{130}Xe (relative to ^{132}Xe) for air are lower than any potential known source, while those of the heavy isotopes ^{134}Xe and ^{136}Xe are higher than any known source (Pepin, 2000; Ozima and Podosek, 2003; Marty et al., 2017). It is not possible to reconstruct the Earth's xenon isotope composition by simple mixing of any combination of nebular ingassed component, chondrite and comet. A number of explanations have been proposedfor the light isotope depletion and heavy isotope enrichment. These include a strong mass-dependent fractionation during hydrodynamic escape (Pepin, 1991; Ozima and Podosek, 2003), or isotope fractionation during ionization with or without the presence of carbonaceous material (Bernatowicz and Fahey, 1986; Hébrard and Marty, 2014; Zahnle et al., 2019). Analyses of Archean age rocks suggests that mass-dependent fractionation may

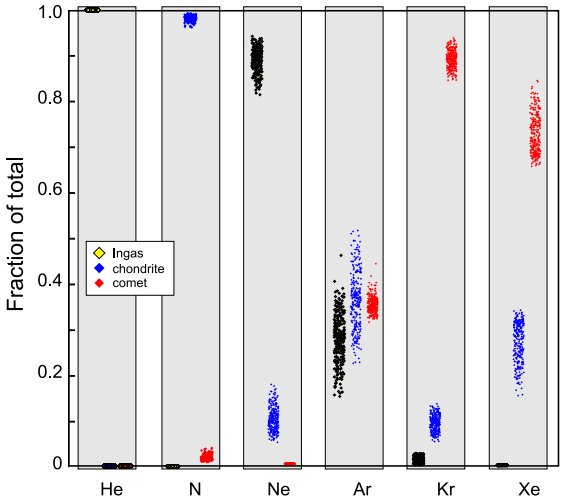

Fig. 2. Relative contributions of volatiles from different sources from 1000 Monte Carlo simulations (420 shown to avoid clutter). The vast majority of He and Ne were supplied by ingassing, whereas N was supplied by chondrites, and Kr and Xe by comets. The higher percentage of Xe and Kr sourced by comets, compared to the light elements He and Ne) is expected due to the formers' higher condensation temperatures.

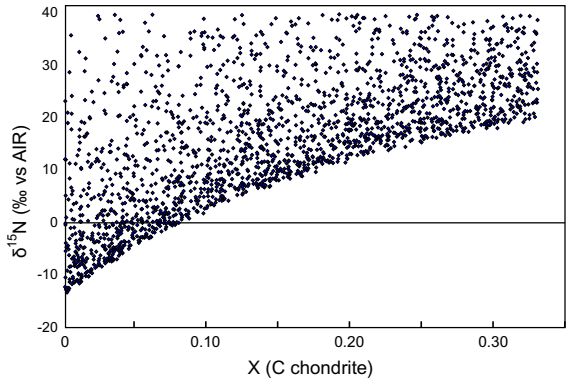

Fig. 4. Calculated $\delta^{15}N$ values of Earth as a function of the C chondrite fraction to the total chondrite addition (C plus E chondrites). No>8% C chondrites is permissible to allow for a less-than-zero $\delta^{15}N$ value for bulk Earth.

have been a long-term process (Avice et al., 2017; Bekaert et al., 2020). A mass dependent Xe loss will deplete the light isotopes and enrich the heavy isotopes relative to an intermediate reference (e.g., ^{130}Xe).

Loss of Xe also affects the Kr/Xe ratios. Bekaert et al. (2020) calculate that 8–12 times the present-day amount of Xe has been lost over the course of Earth history. Our best estimates are 3.5–6.2 (1σ error) time present-day amounts lost (Table 2).

In order to estimate the Xe isotope composition of our simulations, we vary the amount of Xe lost by hydrodynamic escape, the mass dependent fractionation associated with loss (α value), and the assumed Xe isotopic composition of comets (*i.e.,* measured in Comet 67P/C-G vs. solar values). The Xe isotope trends for 400 calculations and for air are shown in Fig. 7. Because the source of Xe to Earth is estimated to be primarily from comets, the calculated overall Xe isotope ratios for Earth are strongly related to the assumed Xe isotope composition of comets. Simulations where the measured (Marty et al., 2017) or calculated (Avice et al., 2020) Xe isotope ratios of Comet 67P/C-G are assumed give Xe isotope ratios that are a poor fit to the Earth values for both heavy and light Xe isotopes. In contrast, our calculated Xe isotope ratios match the Earth values when a presumed solar value is used for the average composition of comets delivered to Earth, and a large mass dependent isotope fractionation during ionized Xe loss is assumed. A mass-dependent fractionation (Fig. 8), using an α value 3 to 5% greater than predicted by Graham's law (where $\alpha = \sqrt{M_1/M_2}$), and M is the mass of the isotopologues fits the Earth data well. Ion implantation

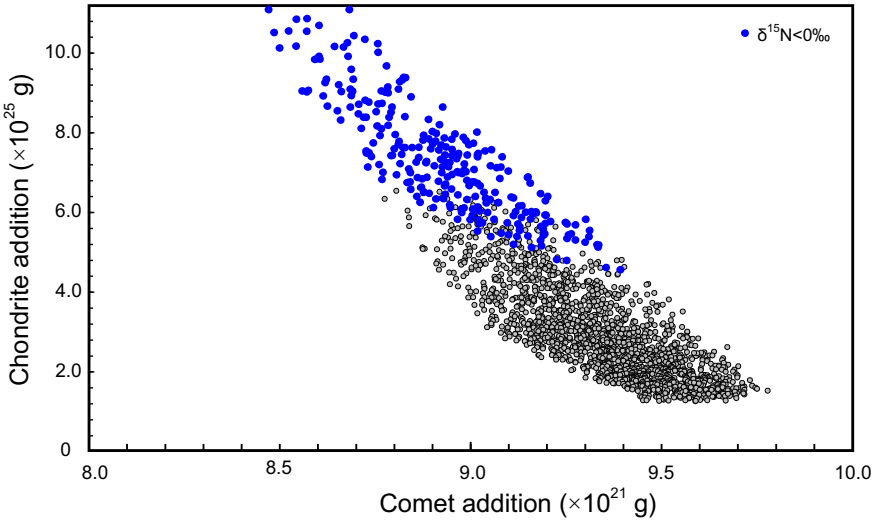

Fig. 3. Chondrite and comet addition estimates from 4000 Monte Carlo simulations. Solutions with $\delta^{15}N$ values < 0‰ require slightly higher chondritic additions and lower cometary additions.

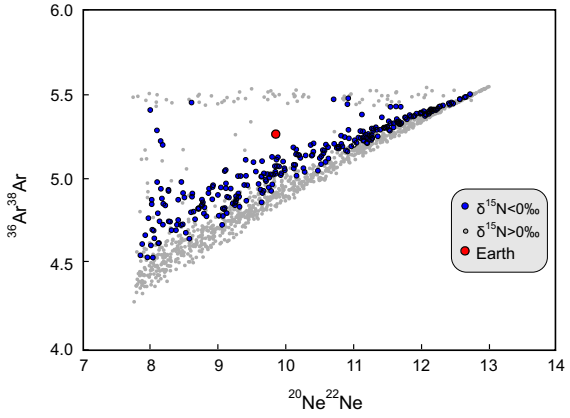

Fig. 5. Ar and Ne isotope ratios from 200 best-fit solutions. The average $^{20}Ne/^{22}Ne$ values of these match Earth, whereas the assumed $^{36}Ar/^{38}Ar$ ratio of Earth show two general trends. The horizontal trend with a value of ~5.5 is obtained when the assumed crossover mass (equation (1)) is less than 38amu. Lower values are obtained for a higher crossover mass.

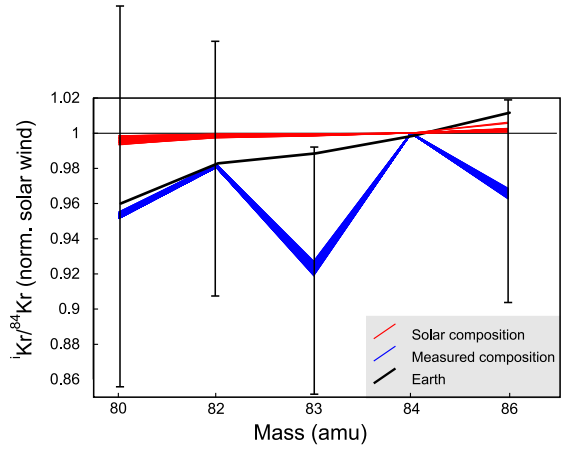

Fig. 6. Kr isotope ratios from 200 best-fit solutions. The Kr isotope data strongly follow the presumed isotopic composition of the cometary source. Solutions using measured cometary compositions from Comet 67P/C-G (blue lines) (Rubin et al., 2018) and assuming a solar cometary compositions (red lines).

experiments (Bernatowicz and Fahey, 1986) result in an isotope fractionation that very closely matches our results which satisfy the overall Xe isotope composition of Earth.

A sample solution that matches the Xe isotope trend and other abundance and isotope ratios is shown in Fig. 8. The results are in good agreement with the average for 400 'best fits' with a large α value for Xe isotope fractionation during ionization and loss.

6.5. Helium

Helium is unique among the noble gases because it is rapidly lost to space. This makes determination of the Earth's original He budget especially difficult, with present-day mantle ^{3}He abundance estimates varying by a factor of 60 (Table 1). We use the median of published

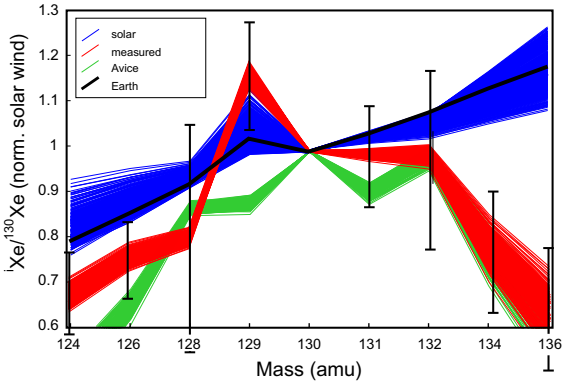

Fig. 7. Results of Monte Carlo simulations for the Xe isotope ratios and the present-day Earth value. Three sets of data were generated. The blue lines are for an assumed solar Xe isotope composition of comets. Red data (measured) are obtained using the measured Xe isotope ratios for Comet 67P/C-G (Marty et al., 2017) and modeled ^{124}Xe and ^{126}Xe from Avice et al. (2020). Green data are obtained using the modeled Xe isotope values of Avice et al. (2020). Blue data are obtained using the solar Xe isotope values as averages for comets. Error bars are for measured Comet 67P/C-G data from Marty et al. (2017).

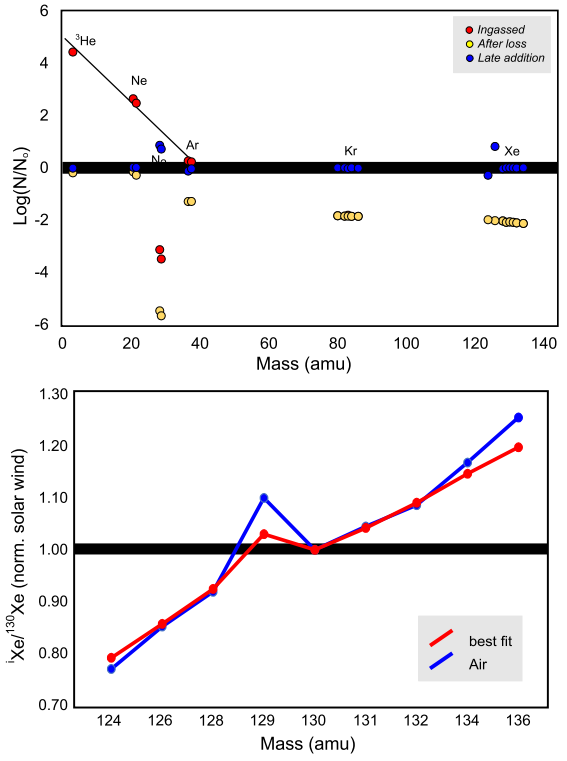

Fig. 8. A solution to ingassed abundance and Xe isotope ratios using data from line 2 of Table 2. Within the uncertainty of input data, all abundances and most isotope ratios match Earth. The Xe isotope composition from our model matches Earth, but only using a mass-dependent α value that is 3% greater than Graham's law estimate where $\alpha = \sqrt{M_1/M_2}$.

values for our present-day estimates, but point out that all proposed values give very similar results in terms of the hydrodynamic escape equation (1) (See Fig. 1).

Although our initial He concentration is considerably higher than previous estimates (Zhang and Zindler, 1989; Porcelli and Elliott, 2008; Dygert et al., 2018), most geochemical systems would not preserve evidence for the early-lost ingassed He.

The importance of ingassing as the source of deep mantle ^{3}He cannot be overstressed. Ingassing is arguably the only method that could effectively deliver abundant ^{3}He to the deep mantle (Porcelli et al., 2001). Late addition from comets or chondrites would most likely not be incorporated into the deep mantle. Experiments suggest that these objects volatilize upon impact (Tyburczy et al., 1986), such that cometary and chondritic-sourced He would be released into the atmosphere and then lost to space.

Olson and Sharp (2022) have postulated that significant He may have dissolved into the core during the early ingassing event. The presence of abundant ^{3}He in the core raises the intriguing possibility that the core may be a major source of ^{3}He for the mantle, not only deep mantle plumes, but also for the He flux at mid-ocean ridges (Porcelli and Halliday, 2001). Core-derived He reduces concerns for retention of deeply sourced mantle ^{3}He that would otherwise be removed by whole-mantle convection.

6.6. Hydrogen

6.6.1. Hydrogen abundance

Hydrogen solubility is silicate melts is strongly dependent on oxygen fugacity ($f(O_2)$), a trait shared with N at low $f(O_2)$ (Libourel et al., 2003; Grewal et al., 2021). Uncertainties in early Earth $f(O_2)$ and subsequent changes that may have occurred during early degassing complicate attempts to quantify hydrogen sources, ingassed amounts and subsequent loss after dissipation of the primordial atmosphere (Sharp, 2017). At the presumed low $f(O_2)$ of Earth's early mantle, the fugacity of H_2 is six times higher than for $f(H_2O)$ (Fig. S1 and supplementary material on details of hydrogen calculations), nevertheless, H in the early magma ocean is predominantly H_2O (or OH^-) rather than molecular H_2 (Fig. 9). For presumed mantle $f(O_2)$ values of IW-2 to IW (where IW is the iron- wüstite buffer – see Appendix A, Supp. Material), our calculated quantity of ingassed H (H_2 and H_2O) to the mantle is 1.6×10^{24} to 3.4×1024 mol H (Fig. 9), corresponding to 11 to 22 ocean equivalents of H_2O. The addition from late addition is at most 10% of the ingassed amount (Table 1 and supplementary material).

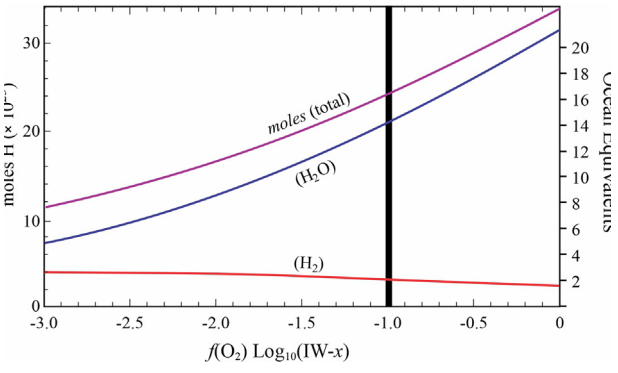

Fig. 9. Amount of ingassed H_2 and H_2O as a function of $f(O_2)$ assuming equilibrium between the mantle and atmosphere and $f(H_2) = 250$ bars, $P_{total} = 280$ bars.

Loss of H_2 by subsequent hydrodynamic escape will raise the $f(O_2)$ of the mantle (Sharp et al., 2013). Loss of 0.5×1024 mol H (as H_2 gas) raises the $f(O_2)$ of the mantle from IW to 1 to FMQ, the presumed present-day mantle $f(O_2)$ (calculations in Supplementary Material and shown in Fig S2). Reduction of H_2O to H_2 (lost) and a concomitant addition of O to the mantle raises the $f(O_2)$. Our calculated $f(O_2)$ increase related to H_2 loss includes the contribution from the mantle iron buffer (Fe^{2+} to Fe^{3+}). Only as $f(O_2)$ approach the FMQ buffer does the iron buffer contribute appreciably to the $f(O_2)$-H_2 loss relationship, because the Fe^{3+}/Fe^{2+} ratio increases only nominally at lower $f(O_2)$ values (Fig. S3).

6.6.2. Hydrogen isotope results

The D/H ratio of Earth is set by the fraction of different components delivered to Earth followed by subsequent loss, either to space during hydrodynamic escape or to the core (Sharp, 2017; Wu et al., 2018). The D/H ratio of material supplied to Earth is estimated from the D/H ratio of each component in proportion to its relative abundance. The D/H ratio of bulk rock E chondrites averages −120‰ (Piani et al., 2020). Comets have variable but high D/H ratios with estimates from 300 to 530 $\times 10^{-6}$ (900–2400‰) (Bockelée-Morvan et al., 2004; Altwegg et al., 2015). The D/H ratio of the solar nebula was very low at 25×10^{-6} (−840‰) (Geiss and Gloeckler, 2003). The amount of H delivered to Earth from these sources gives a D/H ratio of ~37.2, or −760‰ relative to VSMOW. Incorporation of H_2O rather than H_2 during nebular ingassing would raise the D/H ratio of the ingassed component, but not by very much given that the temperatures at the surface of proto-Earth were very high (Olson and Sharp, 2019) and the fractionation between H_2O and H_2 would not have been substantial.

Fractionation associated with subsequent outgassing would raise the D/H ratio. If we assume that atomic hydrogen was the dominant species lost from the early atmosphere (Lammer et al., 2014), then extreme fractionation could occur. The isotope fractionation factor between H_2 and H ranges from $\alpha = 2.56$ at 100 °C to 1.37 at 600 °C (Richet et al., 1977). Rayleigh fractionation with a high α value could bring the δD value of the upper mantle and surface reservoir to its present-day value of ~−40‰. A significantly higher α value of 2.9 would be realized if H rather than H_2 was the species lost to space because the $\alpha_{H_2O\text{-}H}$ value at 300 °C is 2.9 (Richet et al., 1977).

7. CONCLUSIONS

In this contribution we have applied a simple forward model for the sources of volatiles to Earth constructed in light of the presumed formation history of the Earth. We consider ingassing, hydrodynamic escape, late additions, and long-term ionized Xe loss to estimate the contributions from nebular ingassing, late-addition from chondrites, and

late addition from comets. By varying input parameters, we are able to fit the present-day abundance of H, He, N, Ne, Ar, Kr and Xe as well as isotopic ratios (Fig. 8). Importantly, we show that volatile sources depend on the element of interest. Our best-fitting solutions include a vast excess of light gases H, He, and Ne delivered to Earth by nebular ingassing, followed by massive subsequent loss during hydrodynamic escape (Fig. 1). These same solutions predict that heavy noble gases and N_2 were primarily supplied by late addition of chondrites and comets, with the vast majoritity of Kr and Xe supplied by comets, and almost all of N supplied by chondrites (Fig. 2). On the basis of constraints from other elemental system, we find that a contribution of at least 30% of the predicted ingas component (Olson and Sharp, 2019) is necessary to supply sufficient Ar to Earth.

Using the assumed Kr/Xe ratio of Earth as a hard constraint, we match the abundance of all volatile elements in Table 1 and infer 2 (1σ) $\times$ 10^{24} g of C chondrite, 7 $\times$ 10^{25} g of E chondrite, and 9 $\times$ 10^{21} g of comet were delivered to Earth by late addition (Fig. 3). Nitrogen isotope constraints (Fig. 4) strongly support a predominantly E chondrite source for this volatile (late addition).

Our model only considers three processes with 6 free parameters (Section 4). Other processes could be added to the model, including sequestration to the core and distinct mantle and atmosphere reservoirs. Nevertheless, our straightforward approach provides a satisfactory result in terms of sources and quantities of ingassed volatile species.

Declaration of Competing Interest

The authors declare that they have no known competing financial interests or personal relationships that could have appeared to influence the work reported in this paper.

ACKNOWLEDGEMENTS

This work was partly funded by NSF grants EAR-1953992 and EAR1135382 to the two authors. We thank Bernard Marty and two anonymous reviewers for their helpful comments and suggestions.

APPENDIX A. SUPPLEMENTARY MATERIAL

Supplementary material to this article can be found online at https://doi.org/10.1016/j.gca.2022.07.007.

REFERENCES

Albarède F. (2009) Volatile accretion history of the terrestrial planets and dynamic implications. *Nature* **461**, 1227–1233.

Albarede F., Ballhaus C., Blichert-Toft J., Lee C.-T., Marty B., Moynier F. and Yin Q.-Z. (2013) Asteroidal impacts and the origin of terrestrial and lunar volatiles. *Icarus* **222**, 44–52.

Alexander C. M. O. D., Bowden R., Fogel M. L., Howard K. T., Herd C. D. K. and Nittler L. R. (2012) The provenances of asteroids, and their contributions to the volatile inventories of the terrestrial planets. *Science* **337**, 721–723.

Alexander R., Pascucci I., Andrews S., Armitage P. and Cieza L. (2014) The dispersal of protoplanetary disks. In *Protostars and Planets VI* (eds. H. Beuther, R. S. Klessen and C. P. Dullemond). University of Arizona Press, pp. 475–496.

Altwegg K., Balsiger H., Bar-Nun A., Berthelier J. J., Bieler A., Bochsler P., Briois C., Calmonte U., Combi M., De Keyser J., Eberhardt P., Fiethe B., Fuselier S., Gasc S., Gombosi T. I., Hansen K. C., Hässig M., Jäckel A., Kopp E., Korth A., LeRoy L., Mall U., Marty B., Mousis O., Neefs E., Owen T., Rème H., Rubin M., Sémon T., Tzou C.-Y., Waite H. and Wurz P. (2015) 67P/Churyumov-Gerasimenko, a Jupiter family comet with a high D/H ratio. *Science* **347**.

Avice G. and Marty B. (2020) Perspectives on atmospheric evolution from noble gase and nitrogen isotopes on Earth, Mars & Venus. *Space Sci. Rev.* **216**, 36.

Avice G., Marty B. and Burgess R. (2017) The origin and degassing history of the Earth's atmosphere revealed by Archean xenon. *Nat. Comm.* **8**, 15455.

Avice G., Moreira M. and Gilmour J. D. (2020) Xenon Isotopes Identify Large-scale Nucleosynthetic Heterogeneities across the Solar System. *Astrophy. J.* **889**, 68.

Bekaert D. V., Broadley M. W. and Marty B. (2020) The origin and fate of volatile elements on Earth revisited in light of noble gas data obtained from comet 67P/Churyumov-Gerasimenko. *Sci. Reports* **10**, 5796.

Benedikt M. R., Scherf M., Lammer H., Marcq E., Odert P., Leitzinger M. and Erkaev N. V. (2020) Escape of rock-forming volatile elements and noble gases from planetary embryos. *Icarus* **347**, 113772.

Bernatowicz T. J. and Fahey A. J. (1986) Xe isotopic fractionation in a cathodeless glow discharge. *Geochim. Cosmochim. Acta* **50**, 445–452.

Bockelée-Morvan D., Crovisier J., Mumma M. J. and Weaver H. A. (2004) The composition of cometary volatiles. In *Comets, 2* (eds. M. C. Festou, H. U. Keller and H. A. Weaver). University of Arizona Press, pp. 391–423.

Bollard J., Connelly J. N., Whitehouse M. J., Pringle E. A., Bonal L., Jørgensen J. K., Nordlund Å., Moynier F. and Bizzarro M. (2017) Early formation of planetary building blocks inferred from Pb isotopic ages of chondrules. *Sci. Adv.* **3**, e1700407.

Caracausi A., Avice G., Burnard P. G., Füri E. and Marty B. (2016) Chondritic xenon in the Earth's mantle. *Nature* **533**, 82–85.

Carlson R. W., Brasser R., Yin Q.-Z., Fischer-Gödde M. and Qin L. (2018) Feedstocks of the Terrestrial Planets. *Space Sci. Rev.* **214**, 121.

Cartigny P. and Marty B. (2013) Nitrogen isotopes and mantle geodynamics: The emergence of life and the atmosphere-crust-mantle connection. *Elements* **9**, 359–366.

Cassata W. S., Zahnle K. J., Samperton K. M., Stephenson P. C. and Wimpenny J. (2022) Xenon isotope constraints on ancient Martian atmospheric escape. *Earth Planet. Sci. Lett.* **580**, 117349.

Chou C.-L. (1978) Fractionation of the siderophile elements in the earth's upper mantle. *Proc. Lunar Planet. Sci. Conf.* **9**, 219–230.

Dauphas N. and Marty B. (2002) Inference on the nature and the mass of Earth's late veneer from noble metals and gases. *J. Geophys. Res.: Planets* **107**, 12-11-12-17.

Dauphas N. and Morbidelli A. (2014) Geochemical and planetary dynamical views on the origin of Earth's atmosphere and oceans. In *Treatise on Geochemistry* (eds. H. D. Holland and K. K. Turekian), second ed. Elsevier, Oxford, pp. 1–35.

Desch S. J. and Connolly H. C. J. (2002) A model of the thermal processing of particles in solar nebula shocks: Application to the cooling rates of chondrules. *Meteor. Planet. Sci.* **37**, 183–207.

Drake M. J. and Righter K. (2002) Determining the composition of the Earth. *Nature* **416**, 39–44.

Dygert N., Jackson C. R. M., Hesse M. A., Tremblay M. M., Shuster D. L. and Gu J. T. (2018) Plate tectonic cycling modulates Earth's $^{3}He/^{22}Ne$ ratio. *Earth Planet. Sci. Lett.* **498**, 309–321.

Fischer-Gödde M. and Kleine T. (2017) Ruthenium isotopic evidence for an inner Solar System origin of the late veneer. *Nature* **541**, 525–527.

Geiss J. and Gloeckler G. (2003) Isotopic Composition of H, He and Ne in the Protosolar Cloud. *Space Sci. Rev.* **106**, 3–18.

Genda H. and Abe Y. (2005) Enhanced atmospheric loss on protoplanets at the giant impact phase in the presence of oceans. *Nature* **433**, 842–844.

Grady M. M. and Wright I. P. (2003) Elemental and isotopic abundances of carbon and nitrogen in meteorites. *Space Sci. Rev.* **106**, 231–248.

Grady M. M., Wright I. P., Carr L. P. and Pillinger C. T. (1986) Compositional differences in enstatite chondrites based on carbon and nitrogen stable isotope measurements. *Geochim. Cosmochim. Acta* **50**, 2799–2813.

Grewal D. S., Dasgupta R., Hough T. and Farnell A. (2021) Rates of protoplanetary accretion and differentiation set nitrogen budget of rocky planets. *Nature Geosci.*.

Halliday A. N. (2013) The origins of volatiles in the terrestrial planets. *Geochim. Cosmochim. Acta* **105**, 146–171.

Harper C. L. and Jacobsen S. B. (1996) Noble gases and Earth's accretion. *Science* **273**, 1814–1818.

Hayashi C., Nakazawa K. and Nakagawa Y. (1985) Formation of the solar system. *Protostars and planets* **II**, 1100–1153.

Heber V. S., Baur H., Bochsler P., McKeegan K. D., Neugebauer M., Reisenfeld D. B., Wieler R. and Wiens R. C. (2012) Isotopic mass fractionatoin of solar wind: Evidence from fast and slow solar wind collected by the Genesis Mission. *Astrophy. J.* **759**, 121.

Hébrard E. and Marty B. (2014) Coupled noble gas–hydrocarbon evolution of the early Earth atmosphere upon solar UV irradiation. *Earth Planet. Sci. Lett.* **385**, 40–48.

Hernandez J., Hartmann L., Megeath T., Gutermuth R., Muzerolle J., Calvet N., Vivas A. K., Briceno C., Allen L., Stauffer J., Young E. and Fazio G. (2007) A Spitzer Space Telescope Study of Disks in the Young σ Orionis Cluster. *Astrophy. J.* **662**, 1067–1081.

Hirschmann M. M. (2016) Constraints on the early delivery and fractionation of Earth's major volatiles from C/H, C/N, and C/S ratios. *Am. Mineral.* **101**, 540–553.

Holland G., Cassidy M. and Ballentine C. J. (2009) Meteorite Kr in Earth's Mantle Suggests a Late Accretionary Source for the Atmosphere. *Science* **326**, 1522–1525.

Hopp T. and Kleine T. (2018) Nature of late accretion to Earth inferred from mass-dependent Ru isotopic compositions of chondrites and mantle peridotites. *Earth Planet. Sci. Lett.* **494**, 50–59.

Hunten D. M., Pepin R. O. and Walker J. C. G. (1987) Mass fractionation in hydrodynamic escape. *Icarus* **69**, 532–549.

Ida S., Yamamura T. and Okuzumi S. (2019) Water delivery by pebble accretion to rocky planets in habitable zones in evolving disks. *Astron. Astrophys.* **624**.

Javoy M. (1998) The birth of the Earth's atmosphere: the behaviour and fate of its major elements. *Chem. Geol.* **147**, 11–25.

Johansen A. and Lambrechts M. (2017) Forming Planets via Pebble Accretion. *Annu. Rev. Earth Planet. Sci.* **45**, 359–387.

Johansen A., Ronnet T., Bizzarro M., Schiller M., Lambrechts M., Nordlund Å. and Lammer H. (2021) A pebble accretion model for the formation of the terrestrial planets in the Solar System. *Sci. Adv.* **7**, eabc0444.

Kleine T. and Walker R. J. (2017) Tungsten isotopes in planets. *Ann. Rev. Earth Planet. Sci.* **45**, 389–417.

Lammer H., Stökl A., Erkaev N. V., Dorfi E. A., Odert P., Güdel M., Kulikov Y. N., Kislyakova K. G. and Leitzinger M. (2014) Origin and loss of nebula-captured hydrogen envelopes from "sub"- to "super-Earths" in the habitable zone of Sun-like stars. *Monthly Notices Roy. Astron. Soc.* **439**, 3225–3238.

Lammer H., Leitzinger M., Scherf M., Odert P., Burger C., Kubyshkina D., Johnstone C., Maindl T., Schäfer C. M., Güdel M., Tosi N., Nikolaou A., Marcq E., Erkaev N. V., Noack L., Kislyakova K. G., Fossati L., Pilat-Lohinger E., Ragossnig F. and Dorfi E. A. (2020) Constraining the early evolution of Venus and Earth through atmospheric Ar, Ne isotope and bulk K/U ratios. *Icarus* **339**, 113551.

Lécuyer C., Gillet P. and Robert F. (1997) The hydrogen isotope composition of seawater and the global water cycle. *Chemical Geology* **145**, 249–261.

Levison H. F., Kretke K. A., Walsh K. J. and Bottke W. F. (2015) Growing the terrestrial planets from the gradual accumulation of submeter-sized objects. *Proc. Nat. Acad. Sci.* **112**, 14180–14185.

Libourel G., Marty B. and Humbert F. (2003) Nitrogen solubility in basaltic melt. Part I. Effect of oxygen fugacity. *Geochim. Cosmochim. Acta* **67**, 4123–4135.

Lodders K. (2003) Solar system abundances and condensation temperatures of the elements. *Astrophy. J.* **591**, 1220–1247.

Marty B. (2012) The origins and concentrations of water, carbon, nitrogen and noble gases on Earth. *Earth Planet. Sci. Lett.* **313–314**, 56–66.

Marty B., Chaussidon M., Wiens R. C., Jurewicz A. J. G. and Burnett D. S. (2011) A ^{15}N-poor isotopic composition for the solar system as shown by Genesis solar wind samples. *Science* **332**, 1533–1536.

Marty B., Avice G., Sano Y., Altwegg K., Balsiger H., Hässig M., Morbidelli A., Mousis O. and Rubin M. (2016) Origins of volatile elements (H, C, N, noble gases) on Earth and Mars in light of recent results from the ROSETTA cometary mission. *Earth Planet. Sci. Lett.* **441**, 91–102.

Marty B., Altwegg K., Balsiger H., Bar-Nun A., Bekaert D. V., Berthelier J.-J., Bieler A., Briois C., Calmonte U., Combi M., De Keyser J., Fiethe B., Fuselier S. A., Gasc S., Gombosi T. I., Hansen K. C., Hässig M., Jäckel A., Kopp E., Korth A., Le Roy L., Mall U., Mousis O., Owen T., Rème H., Rubin M., Sémon T., Tzou C.-Y., Waite J. H. and Wurz P. (2017) Xenon isotopes in 67P/Churyumov-Gerasimenko show that comets contributed to Earth's atmosphere. *Science* **356**, 1069–1072.

McCubbin F. M. and Barnes J. J. (2019) Origin and abundances of H_2O in the terrestrial planets, Moon, and asteroids. *Earth Planet. Sci. Lett.* **526**, 115771.

Meshik A., Mabry J., Hohenberg C., Marrocchi Y., Pravdivtseva O., Burnett D. S., Olinger C., Wiens R. C., Reisenfeld D. B., Allton J., McNamara K., Stansbery E. and Jurewicz A. J. G. (2007) Constraints on neon and argon isotopic fractionation in solar wind. *Science* **318**, 433–435.

Moreira M. (2013) Noble gas constraints on the origin and evolution of Earth's volatiles. *Geochem. Persp.* **2**, 1–403.

Moreira M., Kunz J. and Allègre C. J. (1998) Rare Gas Systematics in Popping Rock: Isotopic and Elemental Compositions in the Upper Mantle. *Science* **279**, 1178–1181.

Moreira M., Blusztajn J., Curtice J., Hart S., Dick H. and Kurz M. D. (2003) He and Ne isotopes in oceanic crust: Implications for noble gas recycling in the mantle. *Earth Planet. Sci. Lett.* **216**, 635–643.

Nanne J. A. M., Nimmo F., Cuzzi J. N. and Kleine T. (2019) Origin of the non-carbonaceous–carbonaceous meteorite dichotomy. *Earth Planet. Sci. Lett.* **511**, 44–54.

O'Brien D. P., Walsh K. J., Morbidelli A., Raymond S. N. and Mandell A. M. (2014) Water delivery and giant impacts in the 'Grand Tack' scenario. *Icarus* **239**, 74–84.

Olson P. L. and Sharp Z. D. (2022) Primordial helium-3 exchange between Earth's core and mantle. *Geochem. Geophys. Geosys.* **23**, e2021GC009985.

Olson P. L. and Sharp Z. D. (2018) Hydrogen and helium ingassing during terrestrial planet accretion. *Earth Planet. Sci. Lett.* **498**, 418–426.

Olson P. L. and Sharp Z. D. (2019) Nebular atmosphere to magma ocean: A model for volatile capture during Earth accretion. *Phys. Earth Planet. Int.* **294**, 18 p.

Ozima M. and Podosek F. A. (2003) *Noble Gas Geochemistry 2018/07l05 ed.*. Cambridge University Press, Cambridge.

Patzer A. and Schultz L. (2002) Noble gases in enstatite chondrites II: The trapped component. *Meteor. Planet. Sci.* **37**, 601–612.

Pearson V. K., Sephton M. A., Franchi I. A., Gibson J. M. and Gilmour I. (2006) Carbon and nitrogen in carbonaceous chondrites: Elemental abundances and stable isotopic compositions. *Meteor. Planet. Sci.* **41**, 1899–1918.

Pepin R. O. (1991) On the origin and early evolution of terrestrial planet atmospheres and meteoritic volatiles. *Icarus* **92**, 2–79.

Pepin R. O. (2000) On the isotopic composition of primordial xenon in terrestrial planet atmospheres. *Space Sci. Rev.* **92**, 371–395.

Péron S., Moreira M., Putlitz B. and Kurz M. D. (2017) Solar wind implantation supplied light volatiles during the first stage of Earth accretion. *Geochem. Perspec. Lett.* **3**, 151–159.

Péron S., Moreira M. and Agranier A. (2018) Origin of Light Noble Gases (He, Ne, and Ar) on Earth: A Review. *Geochem. Geophys. Geosys.* **19**, 979–996.

Piani L., Marrocchi Y., Rigaudier T., Vacher L. G., Thomassin D. and Marty B. (2020) Earth's water may have been inherited from material similar to enstatite chondrite meteorites. *Science* **369**, 1110–1113.

Porcelli D. and Ballentine C. J. (2002) Models for distribution of terrestrial noble gases and evolatuion of the atmosphere. *Rev. Mineral. Geochem.* **47**, 411–480.

Porcelli D. and Elliott T. (2008) The evolution of He Isotopes in the convecting mantle and the preservation of high $^{3}He/^{4}He$ ratios. *Earth Planet. Sci. Lett.* **269**, 175–185.

Porcelli D. and Halliday A. N. (2001) The core as a possible source of mantle helium. *Earth Planet. Sci. Lett.* **192**, 45–56.

Porcelli D., Woolum D. and Cassen P. (2001) Deep Earth rare gases: initial inventories, capture from the solar nebula, and losses during Moon formation. *Earth Planet. Sci. Lett.* **193**, 237–251.

Pujol M., Marty B. and Burgess R. (2011) Chondritic-like xenon trapped in Archean rocks: A possible signature of the ancient atmosphere. *Earth Planet. Sci. Lett.* **308**, 298–306.

Richet P., Bottinga Y. and Javoy M. (1977) A review of hydrogen, carbon, nitrogen, oxygen, sulphur, and chlorine stable isotope fractionation among gaseous molecules. *Ann. Rev. Earth Planet. Sci.* **5**, 65–110.

Robert F. (2001) The origin of water on Earth. *Science* **293**, 1056–1058.

Robert F., Gautier D. and Dubrulle B. (2000) The Solar System D/H ratio: Observations and theories. *Space Sci. Rev.* **92**, 201–224.

Roth A. S. G., Liebske C., Maden C., Burton K. W., Schönbächler M. and Busemann H. (2019) The primordial He budget of the Earth set by percolative core formation in planetesimals. *Geochem. Persp. Lett.* **9**, 26–31.

Rubin M., Altwegg K., Balsiger H., Bar-Nun A., Berthelier J.-J., Briois C., Calmonte U., Combi M., De Keyser J., Fiethe B., Fuselier A., Gasc S., Gombosi T. I., Hansen K. C., Kopp E., Korth A., Laufer D., Le Roy L., Mall U., Marty B., Mousis O., Owen T., Rème H., Sémon T., Tzou C.-Y., Waite J. H. and Wurz P. (2018) Krypton isotopes and noble gas abundances in the coma of comet 67P/Churyumov-Gerasimenko. *Sci. Adv.* **4**, eaar6297.

Safronov V.S., 1972. Evolution of the protoplanetary cloud and formation of the earth and the planets. Israel Program for Scientific Translations **NASA TTF-677**, 206.

Schiller M., Bizzarro M. and Siebert J. (2020) Iron isotope evidence for very rapid accretion and differentiation of the proto-Earth. *Sci. Adv.* **6**, eaay7604.

Sekiya M., Nakazawa K. and Hayashi C. (1980) Dissipation of the rare gases contained in the primordial Earth's atmosphere. *Earth Planet. Sci. Lett.* **50**, 197–201.

Sharp Z. D. (2017) Nebular ingassing as a source of volatiles to the Terrestrial planets. *Chem. Geol.* **448**, 137–150.

Sharp Z. D., McCubbin M. and Shearer C. K. (2013) A hydrogen-based oxidation mechanism relevant to planetary formation. *Earth Planet. Sci. Lett.* **380**, 88–97.

Trieloff M., Kunz J., Clague D. A., Harrison D. and Allègre C. J. (2000) The nature of pristine noble gases in mantle plumes. *Science* **288**, 1036–1038.

Tyburczy J. A., Frisch B. and Ahrens T. J. (1986) Shock-induced volatile loss from a carbonaceous chondrite: implications for planetary accretion. *Earth Planet. Sci. Lett.* **80**, 201–207.

Villeneuve J., Chaussidon M. and Libourel G. (2009) Homogeneous Distribution of ^{26}Al in the Solar System from the Mg Isotopic Composition of Chondrules. *Science* **325**, 985–988.

Walker R. J. (2009) Highly siderophile elements in the Earth, Moon and Mars: Update and implications for planetary accretion and differentiation. *Chem. Erde* **69**, 101–125.

Walker R. J., Horan M. F., Morgan J. W., Becker H., Grossman J. N. and Rubin A. E. (2002) Comparative ^{187}Re-^{187}Os systematics of chondrites: Implications regarding early solar system processes. *Geochim. Cosmochim. Acta* **66**, 4187–4201.

Walsh K. J. and Levison H. F. (2016) Terrestrial planet formation from an annulus. *Astrophys. J.* **152**, 68.

Wetherill G. W. (1980) Formation of the Terrestrial Planets. *Ann. Rev. Astron. Astrophys.* **18**, 77–113.

Williams C. D. and Mukhopadhyay S. (2018) Capture of nebular gases during Earth's accretion is preserved in deep mantle neon. *Nature* **565**, 78–81.

Wu J., Desch S. J., Schaefer L., Elkins-Tanton L. T., Pahlevan K. and Buseck P. R. (2018) Origin of Earth's Water: Chondritic Inheritance Plus Nebular Ingassing and Storage of Hydrogen in the Core. *J. Geophys. Res.: Planets* **123**, 2691–2712.

Yokochi R. and Marty B. (2004) A determination of the neon isotopic composition of the deep mantle. *Earth Planet. Sci. Lett.* **225**, 77–88.

Zahnle K. J., Gacesa M. and Catling D. C. (2019) Strange messenger: A new history of hydrogen on Earth, as told by Xenon. *Geochim. Cosmochim. Acta* **244**, 56–85.

Zahnle K. J. and Kasting J. F. (1986) Mass fractionation during transonic escape and implications for loss of water from Mars and Venus. *Icarus* **68**, 462–480.

Zhang Y. and Zindler A. (1989) Noble gas constraints on the evolution of the Earth's atmosphere. *J. Geophys. Res.: Solid Earth* **94**, 13719–13737.

Zhu M.-H., Morbidelli A., Neumann W., Yin Q.-Z., Day J. M. D., Rubie D. C., Archer G. J., Artemieva N., Becker H. and Wünnemann K. (2021) Common feedstocks of late accretion for the terrestrial planets. *Nature Astron.* **5**, 1286–1296.

Associate editor: Manuel Moreira